Supplementary Information for

Surface precleaning strategy intensifies interface coupling of Bi_2O_3/TiO_2 heterostructure for enhanced photoelectrochemical detection properties

*Yajun Pang[a, b, #], Qiang Feng[a, #], Zongkui Kou[b, *], Guangqing Xu[a, c, *], Feng Gao[a], bo Wang[a], Zhenghui Pan[b], Jun Lv[a, c], Yong Zhang[a, c], Yucheng Wu[a, c]*

[a] School of Materials Science and Engineering, and Key Laboratory of Advanced Functional Materials and Devices of Anhui Province, Hefei University of Technology, Hefei 230009, China.

[b] Department of Materials Science and Engineering, National University of Singapore, Singapore 117574, Singapore.

[c] China International S&T Cooperation Base for Advanced Energy and Environmental Materials, Hefei 230009, China.

*Corresponding authors. E-mail: msekz@nus.edu.sg (**Z. Kou**); gqxu1979@hfut.edu.cn (**G. Xu**).

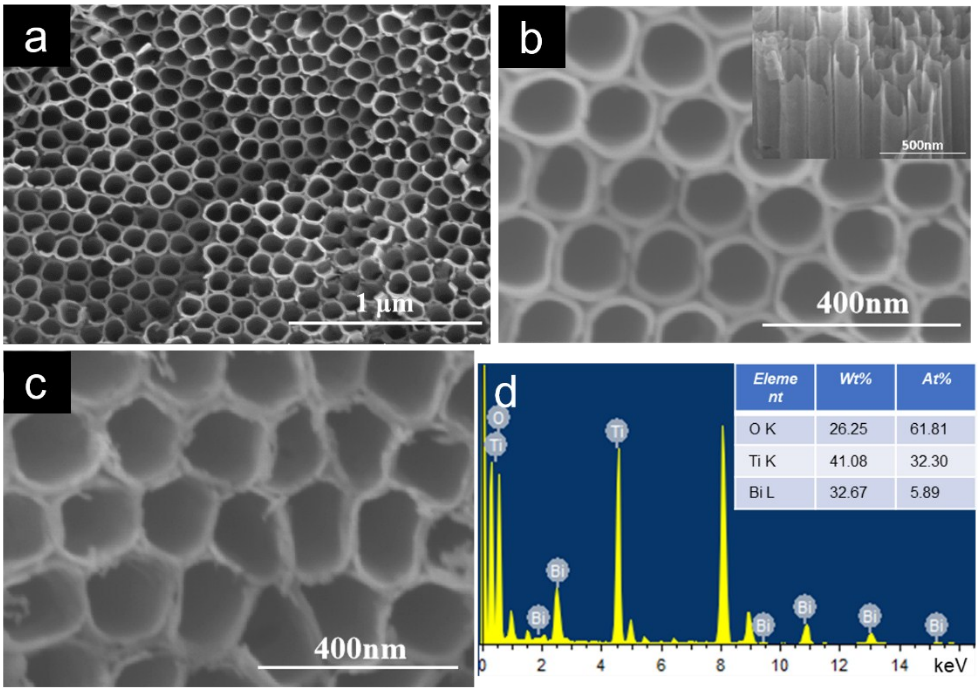

Figure S1. SEM images of (a) TiO_2, (b) *c*-TiO_2, (c) Bi_2O_3/*c*-TiO_2 for 1 cycle, and (d) EDS spectrum from TEM image of Bi_2O_3/*c*-TiO_2.

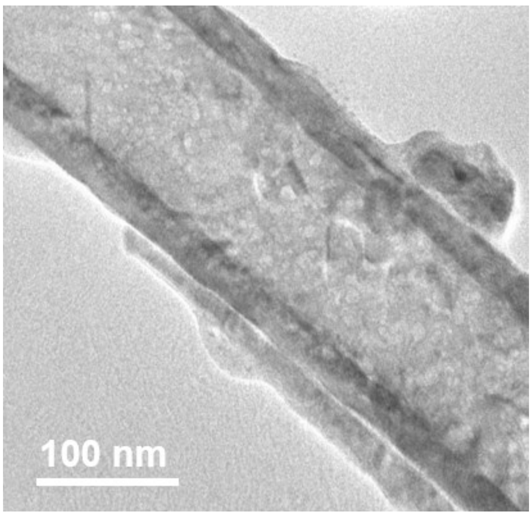

Figure S2. TEM image of a single TiO_2 nanotube.

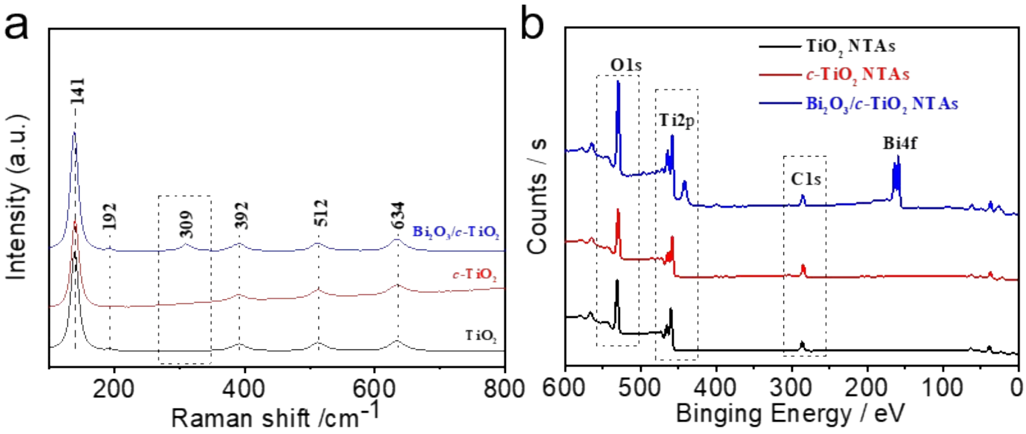

Figure S3. Raman spectra (a) and XPS Survey patterns (b) of TiO_2, *c*-TiO_2, and Bi_2O_3/*c*-TiO_2 NTAs.

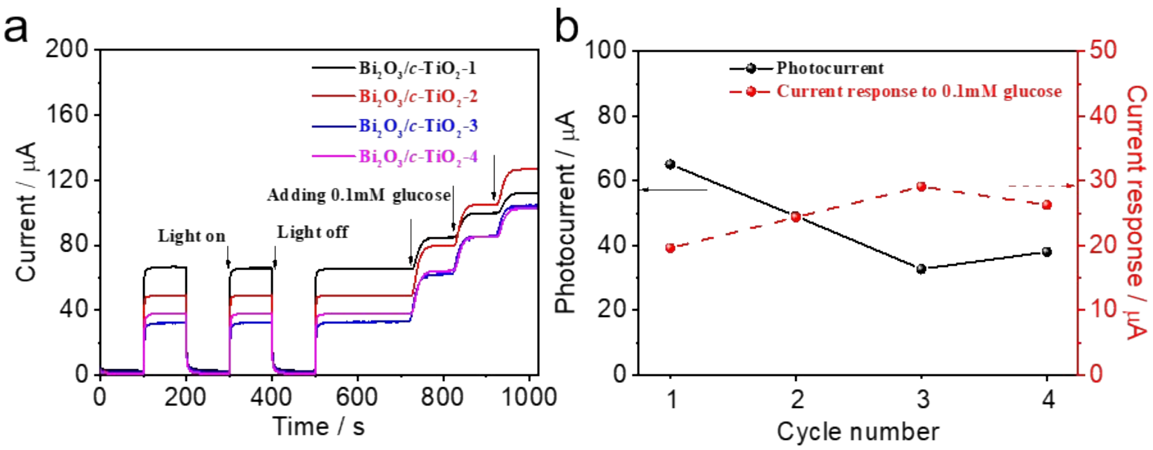

Figure S4. Photocurrents and current response of Bi_2O_3/*c*-TiO_2 NTAs with different cycles: (a) current-time curves, (b) plots of photocurrent and current response *vs.* deposition cycle.

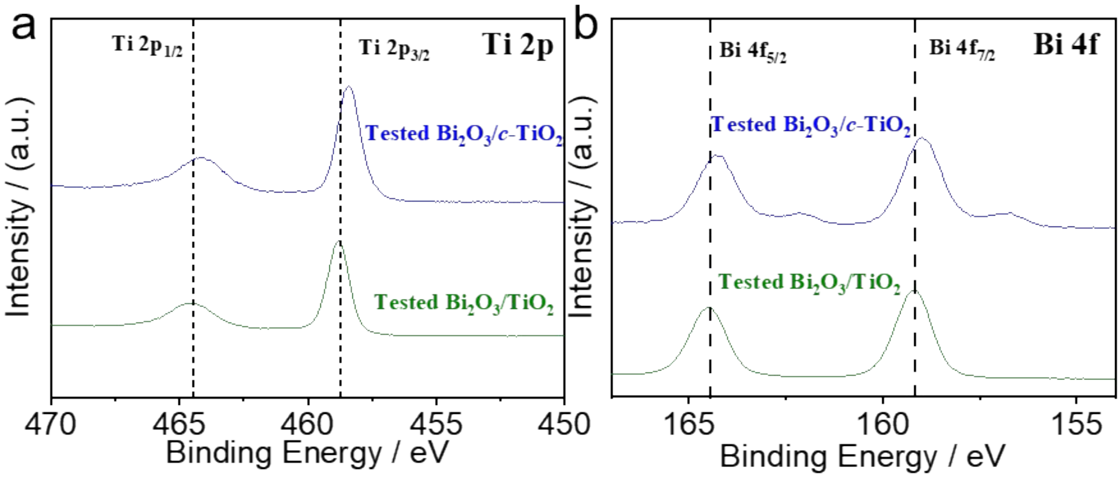

Figure S5. High resolution XPS spectrum of Ti 2p and Bi 4f spectrum for the tested Bi_2O_3/TiO_2 and Bi_2O_3/c-TiO_2 respectively.

Table S1. Detection parameters of TiO_2, *c*-TiO_2, Bi_2O_3/TiO_2, and Bi_2O_3/c-TiO_2 NTAs.

Composite	Current noise μA	Sensitivity μA/(μM)	Linear range μM	Limit of Detection * μM
TiO_2	0.812	0.088	985.8	27.68
c-TiO_2	0.431	0.142	888.1	8.37
Bi_2O_3/TiO_2	0.669	0.162	1088.03	12.39
Bi_2O_3/ *c*-TiO_2	0.372	0.214	1185.5	5.21

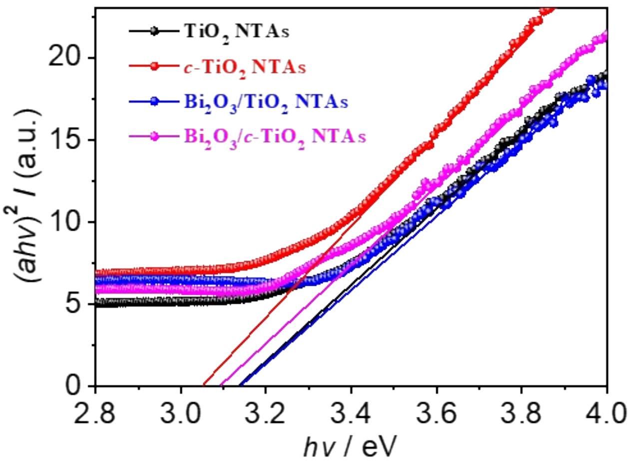

Figure S6. Transformed Kubelka−Munk function versus photon energy curves of TiO_2, c-TiO_2, Bi_2O_3/TiO_2, and Bi_2O_3/c-TiO_2 NTAs, respectively.

Transformed Kubelka−Munk function versus photon energy curves were applied to investigate the band gap of as-obtained four samples (**Figure S6**). Thereby, on the one hand, compared with TiO_2, the Eg of c-TiO_2 is reduced with the low temperature hydrogen thermal treatment; on the other hand, the Eg of Bi_2O_3/c-TiO_2 is obviously changed when compared with c-TiO_2, while there is no much difference between the Bi_2O_3/TiO_2 and TiO_2, which further proves that such an surface precleaning strategy can greatly facilitate the strong coupling in Bi_2O_3/c-TiO_2 NTAs.